J Mater Sci (2011) 46:7298–7312
DOI 10.1007/s10853-011-5691-5

Molecular-level analysis of shock-wave physics and derivation of the Hugoniot relations for soda-lime glass

M. Grujicic · B. Pandurangan · W. C. Bell · B. A. Cheeseman · P. Patel · G. A. Gazonas

Received: 12 October 2010 / Accepted: 4 June 2011 / Published online: 17 June 2011

Abstract Non-equilibrium and equilibrium molecular dynamics simulations are employed to study the mechanical response of soda-lime glass (a material commonly used in transparent armor applications) when subjected to the loading conditions associated with the generation and propagation of planar shock waves. Particular attention is given to the identification and characterization of various (inelastic-deformation and energy-dissipation) molecular-level phenomena and processes taking place at the shock front. The results obtained revealed that the shock loading causes a 2–4% (shock strength-dependent) density increase. In addition, an increase in the average coordination number of the silicon atoms is observed along with the creation of smaller Si–O rings. These processes are associated with significant energy absorption and dissipation and are believed to control the blast/ballistic impact mitigation potential of soda-lime glass. This study was also aimed at the determination (via purely computational means) of the shock Hugoniot (i.e., a set of axial stress vs. density/specific-volume vs. internal energy vs. particle velocity vs. temperature) material states obtained in soda-lime glass after the passage of a shock wave of a given strength and on the comparison of the computed results with their experimental counterparts. The availability of a shock Hugoniot is critical for construction of a high deformation-rate, large-strain, high pressure material model which can be used within a continuum-level computational analysis to capture the response of a soda-lime glass-based laminated transparent armor structure (e.g., a military vehicle windshield, door window, etc.) to blast/ballistic impact loading.

M. Grujicic (✉) · B. Pandurangan · W. C. Bell
Department of Mechanical Engineering,
Clemson University, 241 Engineering Innovation Building,
Clemson, SC 29634-0921, USA
e-mail: gmica@exchange.clemson.edu

B. A. Cheeseman · P. Patel · G. A. Gazonas
Army Research Laboratory—Survivability Materials Branch,
Aberdeen, Proving Ground, MD 21005-5069, USA

Introduction

While novel transparent ceramics and transparent polymeric materials are being increasingly used in various blast/ballistic-impact resistant vehicle transparent structures (e.g., windshields, door windows, viewports, etc.), ballistic glass remains an important material component in these structures [1, 2]. The main reasons for this have been discussed in great detail in our recent work [3–6].

Typically, the development of new glass-based transparent impact resistant structures involves extensive prototyping and laboratory/field experimental testing. While these experimental efforts are critical for ultimate validation of the transparent impact resistant structures, they are generally expensive, time-consuming, and involve destructive test procedures. In addition, it is well-established (e.g., [3–6]) that the effectiveness and reliability of the computation-based modeling and simulation approaches is strongly correlated with the fidelity of the associated material models. In other words, it is critical that these models realistically describe deformation/fracture response of the subject material (ballistic glass, in the present case) under high-rate, large-strain, high-pressure loading conditions encountered during blast/ballistic impact. Therefore, one of the main objectives of this study is to explore the possibility for using molecular-level computational simulations to improve fidelity of the models representing the material under consideration. Specifically, phenomena and

processes accompanying the formation and propagation of shock-waves within soda-lime glass will be investigated to derive the associated functional relations between different material state variables.

A comprehensive literature review carried out as part of our prior work [6] revealed that the mechanical behavior of glass is modeled predominantly using three distinct approaches: (a) molecular-modeling methods [7–10], (b) continuum-material approximations [3–6, 11–14], and (c) models based on explicit crack representation [15, 16]. In addition, this review established that only the molecular-level models are capable of identifying nanometer length scale phenomena and the associated microstructure evolution processes accompanying high-rate deformation of soda-lime glass. This is the main reason that molecular-level methods and tools are employed in this study.

As mentioned above, the main objective of this study is to investigate various shock-wave-related phenomena using molecular-level computational methods.

A shock wave (or simply a shock) is a wave which propagates through a medium at a speed higher than the sound speed and its passage causes an abrupt and discontinuous change in the material state variables (e.g., pressure, internal energy, density, temperature, and particle velocity). The magnitude of the state-variable changes and the shock speed increases with the strength of the shock. In reality, since no material can support a discontinuity in its state variables, shocks manifest themselves as continuous (structured) waves with a steep and narrow wave front. While acoustic waves give rise to isentropic changes in the material state variables, passage of a shock is typically associated with irreversible (entropy-increasing) changes in the same variables. The reason behind this difference is that shock involves very high strain rates that bring energy-dissipative viscous effects into prominence.

Based on an open-literature review, conducted as part of this study, it was established that molecular-level computational methods were first employed to study shocks more than 30 years ago [17–20]. While the initial focused on shock phenomena in dense fluids, subsequent analyses were extended to single-crystalline solids. The key findings related to the generation and propagation of shocks in the single-crystalline solids investigated can be summarized as follows: (a) shock-wave phenomena are inherently more complex in solids than in fluids, because solids, in addition to the lattice parameter, introduce a new length scale (i.e., the size/spacing of defects) which tends to control the nature/extent of inelastic-deformation processes (mainly responsible for energy dissipation at the shock front), (b) initial (un-steady) shock waves tend to become steady (time-invariant) as they propagate and this process is facilitated by the transverse displacement of atoms which produce inelastic deformations. These deformation involves concerted slippage of atoms over each other and is not dominated by viscous flow as in the case of shocks in fluids, and (c) in order to eliminate free-surface effects and model bulk-material behavior, molecular-level modeling of shock is typically carried out using computational systems with periodic boundary conditions (at least in directions transverse to the shock-wave propagation direction). As a consequence of the use of the periodic boundary conditions within shock-wave molecular-level simulations, a single shock (or often a pair of converging shocks) is associated with each computational cell. To attain steady wave conditions of the shock, computational domains sufficiently long in the direction of shock-wave propagation have to be employed. For a typical 5000–7000 m/s range of the shock speed and a typical 20 ps computation time the minimum computational-cell length required is of the order of 100–150 nm. It should be also noted that, lateral dimensions of the computational domain have to be also sufficiently large to avoid spurious effects associated with the use of the periodic boundary conditions. Consequently, computational domains involving several tens of thousands of atoms have to be employed in shock-wave simulations requiring prolonged wall-clock simulation times. Furthermore, since weak and moderate shocks in single crystalline solids can have width on the order of 100–500 nm they could not be readily modeled using the molecular-level methods. However, as will be shown in this study, when the energy dissipative mechanisms are not very potent (as is the case in soda-lime glass), moderate shocks are associated with significantly smaller width and they could be studied using molecular-level methods.

As mentioned earlier, a preliminary molecular-level computational study of shock generation/propagation in soda-lime glass is carried out in this study. The study has the following two main objectives:

(a) To determine the shock Hugoniot (centered on the initial stress-free quiescent state) of soda-lime glass. A Hugoniot is the locus of axial stress versus specific volume versus energy density (vs. particle velocity vs. shock speed) shocked ("upstream") material states. The Hugoniot is often used in the derivation of the continuum-level material models of the type employed in transient non-linear dynamics analyses of the response of structures to shock loading. In situations in which one is interested only in the problem of planar shock propagation/interaction (in the presence of uni-axial strain deformation states), a complete definition of the continuum-level material model is not required. Instead, the knowledge of the corresponding Hugoniots (i.e., Hugoniot functional relations) is sufficient; and

(b) The Hugoniot relations mentioned in (a) provide a global statement of mass, momentum, and energy conservation accompanying shock-induced material transition from a given initial ("downstream") equilibrium state to all possible final ("upstream") equilibrium states for steady planar shock waves (of different strengths). However, these relations provide no information about the structure of the shock front or the nature of the dissipative structural rearrangement mechanisms that lead to the formation of a steady shock wave. Hence, the second objective of this study is to carry out a detailed examination of the downstream, shock-front, and upstream material states (as represented by the local stresses, strains, densities/specific volumes, temperatures, etc.) and molecular-level morphology to identify and characterize these processes.

The organization of the article is as follows: A brief description of the molecular-level microstructure of glass including its random-network representation is presented in second section. A brief overview of the molecular-level computational procedure including the computational cell construction, force field identification, computational method(s) selection, shock-wave generation, and the problem definition are, respectively presented in third section. The key results obtained in this study are presented and discussed in fourth section. A summary of the study carried out and the key results/conclusions are given in fifth section.

Molecular-level microstructure of glass

One of the basic properties of all glass-like materials is their lack of long-range atomic order which classifies them as amorphous materials. For instance, the atomic arrangement in pure silicate glass (i.e., fused silica) is highly random relative to the crystalline Si–O modifications like quartz or cristobalite. To describe the random atomic arrangement within glass the so-called random network model [21] is typically employed. Such a model represents amorphous materials as a three-dimensional linked network of polyhedra with central cations of various coordinations depending on the character of the atomic constituents. In the case of silicate-based glasses like fused silica and soda-lime glass, the polyhedral central cation is silicon. In this case, each silicon is surrounded by four oxygen anions and forms a SiO_4^{4-} tetrahedron, whereby each oxygen is bonded to (or bridges) two silicon atoms. Other polyhedra may exist in the network depending on the valence of the added polyhedral-center cations.

Ceramic glasses like soda-lime glass investigated in this study are generally a mixture of various oxides. Oxide constituents of the ceramic glasses are generally classified as: (a) *Network formers* oxides (e.g., SiO_2, B_2O_3, GeO_2) falling into this category have the tendency to form a continuous network with "bridging" oxygen atoms; and (b) *Network modifiers* oxides falling into this category are typically based on alkali (e.g., Na, K, etc.) and alkaline earth (e.g., Ca, Mg, etc.) metals. In the specific case of soda-lime glass, investigated in this study, the 14 wt% Na_2O and 9 wt% CaO additions pure SiO_2 glass both act as network modifiers. When alkali/alkaline earth metal-based oxides are added to pure SiO_2 glass, excess oxygen which results from the ionic dissociation of these oxides is incorporated into the glass network. This process disrupts network continuity since it replaces single continuity-forming bridging oxygen atom with two (network-breaking) singly charged non-bridging oxygen ions. The latter oxygen ions are the result of charge transfer from the initially double charged oxygen ions (produced during dissociation of alkali/alkaline earth metal-based oxides) to the initially neutral bridging oxygen atoms. The metallic cations formed during dissociation tend to hover around the non-bridging oxygen ions for local charge neutrality.

Within the random network model, the microstructure of glass is described using several network state parameters. Among these, the most frequently used are: (a) the so-called R parameter, defined as the average number of oxygen ions per network forming cation. In a glass of a given chemistry, this parameter is effectively microstructure-insensitive since its value depends solely on the chemical composition of glass. For example, in the case of fused silica, in which there are two oxygen anions for every network forming silicon cation, the R value is 2.0. On the other hand, in the case of soda-lime glass, the introduction of additional oxygen ions (without the introduction of additional network forming cations) causes the R value to increase to ca. 2.41. In accordance with the earlier discussion regarding the role of glass modifiers, it is apparent that a larger value of the R parameter implies a more open, weaker glass network. The effect of network formers on the R parameter is more complicated and depends on the network former coordination number as well as its concentration. Overall the R parameter is a measure of the maximum extent of connectivity that can be achieved within a glass of a given chemistry. It should be noted that since shock loading is assumed to only produce physical/microstructural changes in glass, the R value is not expected to change during shock loading; (b) the so-called X parameter which defines the average number of non-bridging (connected to only a single network forming cation) oxygen atoms per network polyhedron. The equilibrium value of this parameter can again be calculated

using the known chemical composition of glass. For example, this parameter takes on a zero equilibrium value in the case of fused silica since all oxygen ions are of a bridging type. However, in the case of soda-lime glass for the reasons mentioned above, the equilibrium value of this parameter is ca. 0.81. It should be noted that shock loading-induced damage in glass will generally increase the number of non-bridging oxygen ions (through Si–O bend breaking), resulting in an increase of the X parameter beyond its equilibrium value; and (c) the so-called Y parameter which defines the average number of bridging (connected to two network forming cations) oxygen atoms per network polyhedron. The equilibrium values for this parameter in fused silica and soda-lime glass are 4.0 and 3.19, respectively. Shock loading will generally lower the value of this parameter below the equilibrium value.

In addition to chemical modifications of glass, changes in the microstructure of this material can be brought about by mechanical loading/deformation (typically requiring several GPa pressure levels). Specifically, high pressure may result in a reorganization of the atomic network (phase change) in the form of changes to the coordination of the network forming cations. These phase changes can be of first order, which are characterized by the formation of a distinct high-pressure phase at a nominally constant pressure, or they may be of second order which are phase changes which involve a continuous morphing of the original phase into the final high-pressure phase over a range of pressures. These phase transformations may be associated with significant volume changes and, since phase-transformation induced energy absorption is a well-documented phenomenon responsible for high toughness levels in TRIP steels and partially stabilized crystalline ceramics, it is of interest to this study.

The phase transformations of glass which are investigated in this study occur in the range of 3–5 GPa. The phase transformations in question have not been fully investigated or characterized in terms of the random network model or using other microstructural parameters. However, the presence of these transformations has been inferred indirectly through the changes in the shock Hugoniot relations for soda-lime glass [22]. These changes typically result in an anomalous stiffness-decreasing response of the material during loading. This pressure range was chosen for the current investigation as it is consistent with the levels seen in glass structures subject to ballistic/blast loading and is associated with relatively modest (3–7%) volume changes. These phase-transformations should not be confused with those seen to take place at substantially higher pressures (ca. >20 GPa), which are considered to be of second order and associated with substantially larger volume reductions and with the formation of stishovite, an octahedrally coordinated glass phase.

Molecular-level analysis of soda-lime glass

As mentioned earlier, molecular-level computational methods have been employed in this study to investigate shock formation and propagation in soda-lime glass. Within these methods, all atoms, ions, and bonds are explicitly accounted for and molecular mechanics, dynamics or Monte Carlo algorithms are used to quantify the behavior of the material under investigation.

While ab initio quantum mechanics methods have the advantage over the molecular-level methods since they do not require parameterization, they have a serious shortcoming. Namely, due to prohibitively high computational cost, they can be currently employed only for systems containing no more than a few hundred atoms/particles. As will be shown below, while ab initio quantum-mechanics calculations are not directly used in this study, some of the computational ab initio quantum mechanics results are used in the parameterization of the material model at the molecular length/time scale. Utility of the molecular-level computational results is greatly dependent on accuracy and fidelity of the employed force field (the mathematical expressions which describe various bonding and non-bonding interaction forces between the constituents of the molecular-level model). In this study, the so-called Condensed-phase Optimized Molecular Potentials for Atomistic Simulation Studies (COMPASS) force field is used [23, 24]. This highly accurate force field is of an ab initio type since most of its parameters were determined by matching the predictions made by the ab initio quantum mechanics calculations to the condensed-matter experimental data. Hence, it should be recognized that the COMPASS force field is a prime example of how the highly accurate results obtained on one length/time scale (quantum mechanic/electronic, in the present case) and the experimental data can be combined to parameterize material models used at coarser length/time scale (the molecular length/time scale, in the present case).

Formulation of a molecular-level simulation problem requires, at a minimum, specification of the following three aspects: (a) a molecular-level computational model consisting of atoms, ions, functional groups, and/or molecules; (b) a set of force field functions; and (c) a computational method(s) to be used in the simulation. More details of these three aspects of the molecular-level modeling and simulation of soda-lime glass are provided below.

Computational model

At the molecular level, soda-lime glass is modeled as a discrete material consisting of (a) silicon (Si) and oxygen (O) atoms mutually bonded via a single covalent bond and forming a connected, non-structured/amorphous network of

silica (SiO_4^{4-}) tetrahedra; (b) oxygen anions (O^{2-}) attached as terminal functional-groups to the fragmented silica tetrahedra network; and (c) sodium cations (Na^+) dispersed between fragmented silica tetrahedra networks and ionically bonded to the oxygen anions.

While glass is an amorphous material and does not possess any long-range regularity in its atomic/molecular structure, modeling of bulk behavior of glass is typically done at the molecular level by assuming the existence of a larger (amorphous) unit cell. Repetition of this cell in the three orthogonal directions (the process also known as application of the "periodic boundary conditions") results in the formation of an infinitely large bulk-type material. This procedure was adopted in this study.

The parallelopiped-shaped computational cell used in this study contained 2,304 particles (Si-512, Na^+-512, O^-256, and O-1024). The computational cell edge-lengths were initially set to $a = 7.471$ nm and $b = c = 1.868$ nm, yielding a soda-lime glass initial nominal density of 2.613 g/cm^3. The three edges (a, b, and c) of the cell were aligned, respectively, with the three coordinate axes (x, y, and z).

To create the initial particle configuration in the unit cell, the Visualizer [25] program from Accelrys was first used to construct a short silica-chain fragment. The fragment was then "grown" by a duplicate-and-attach process using the same program. The resulting silica network (along with additional sodium cations and oxygen anions) was next used within the Amorphous Cell program [26] from Accelrys to randomly populate the computational cell while ensuring that the target material density of 2.613 g/cm^3 was attained. An example of a typical molecular-level topology within a single unit cell is displayed in Fig. 1.

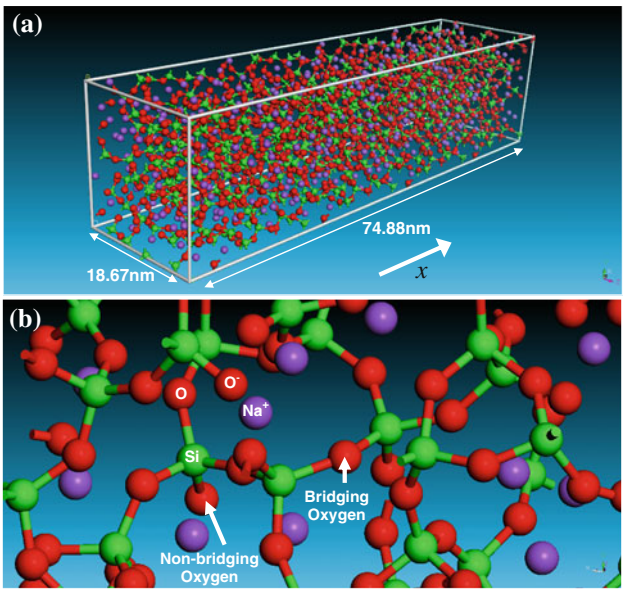

Fig. 1 **a** The computational unit cell for soda-lime glass molecular-level simulations used in this study; and **b** an example of the local atomic structure (Color figure online)

Force-fields

As stated above, the behavior of a material system at the molecular-level is governed by the appropriate force-fields which describe, in an approximate manner, the potential energy hyper-surface on which the atomic nuclei move. In other words, the knowledge of force-fields enables determination of the potential energy of a system in a given configuration. In general, the potential energy of a system of interacting particles can be expressed as a sum of the valence (or bond), cross-term and non-bond interaction energies. Each of these energy components, in turn, contains a number of subcomponents. For example, the valence energy contains the contributions from single bond stretching, two-bond angle changes, three-bond dihedral bond angle changes, etc. The cross energy term includes the contributions from the interactions of the subcomponents of the valence terms (e.g., stretch/stretch interaction, stretch/bond-angle change interaction, etc.). The non-bond interaction term accounts for the interactions between non-bonded atoms and includes the van der Waals energy and the Coulomb electrostatic energy.

As mentioned earlier, the present molecular-level analysis of soda-lime glass employs the COMPASS [23, 24] force-field for various bond and non-bond interaction energies. A summary of the COMPASS force-field functions can be found in our previous study [27].

Computational method

Both molecular statics and molecular dynamics simulations were employed in this study. Within the molecular statics approach, the unit-cell potential energy is minimized with respect to the position of the constituent particles/atoms. The potential energy minimization within Discover [28] (the atomic simulation program from Accelrys used in this study) is carried out by combining the Steepest Descent, Conjugate Gradient, and the Newton's minimization algorithms. These algorithms are automatically inactivated/activated as the atomic configuration is approaching its energy minimum (i.e., the Steepest Descent method is activated at the beginning of the energy minimization procedure while the Newton's method is utilized in the final stages of this procedure).

As will be discussed in greater detail in section "Results and discussion," molecular statics is employed to determine the state of the material swept by a shock. As will be shown, this procedure is based on the use of (bonding and non-bonding) potential energy components and neglects

shock-induced changes in the (configurational) entropy of the system. To assess the consequence of this simplification, the approach described in [29] was considered. This approach defines a dimensionless parameter and states that when this parameter is significantly smaller than unity, entropy effects can be neglected. Unfortunately, detailed temperature and pressure dependencies of the material mechanical response of soda-lime glass needed to evaluate this parameter were not available with sufficient fidelity. Hence, the results obtained by the application of this procedure, which suggest that the entropy effects may not be highly critical, cannot be accepted with a high level of confidence.

Within the molecular dynamics approach, gradient of the potential energy with respect to the particle positions is first used to generate forces acting on the particles and, then, the associated Newton's equations of motion (for all particles) are integrated numerically to track the temporal evolution of the particle positions. Both the equilibrium and the non-equilibrium molecular dynamics methods are employed in this study. Within the equilibrium molecular-dynamics methods, the system under consideration is coupled to an (external) environment (e.g., constant pressure piston, constant temperature reservoir, etc.) which ensures that the system remains in equilibrium (i.e., the system is not subjected to any thermodynamic fluxes). As will be discussed in next section, *NVT* [where N is the (fixed) number of atoms, V, the computational cell volume (also fixed), and T(=298 K) is the temperature] equilibrium molecular dynamics is employed in the first stage of the shock generation procedure. In addition, as will be discussed in section "Results and discussion", *NVE* (E is the total energy) equilibrium molecular dynamics is also employed during determination of the shock Hugoniot. Within non-equilibrium molecular dynamics, the system is subjected to large perturbations (finite changes in the axial parameter of the computational cell, in the present case) which create a thermodynamic flux (i.e., the flux of energy and momentum, in the present case). More details regarding the use of Discover to carry out molecular statics and molecular dynamics analyses can be found in our prior study [6].

Shock-wave generation

To generate a planar shock (or more precisely a pair of planar shocks) within the computational cell, the following procedure is employed:

(a) At the beginning of the analysis, a "sufficiently long" *NVT* molecular dynamics simulation is carried out to equilibrate the system/material.

(b) The shock is then initiated (and driven) by continuously contracting the computational cell x-direction lattice parameter a as:

$$a(t) = a(t = 0) - 2u_p t \tag{1}$$

where t denotes time, u_p is the so-called piston velocity (or equivalently the particles upstream velocity) in the x-direction. u_p is varied over a range between 187.5 and 1500 m/s to simulate the generation and propagation of shock of various strengths. Meanwhile, computational-cell transverse lattice parameters b and c are kept constant to obtain planar (uniaxial-strain) shock conditions. In this process, the computational cell faces normal to the shock propagation-direction behave very similarly to the impact-surface of a plate-like target subjected to a so-called symmetric "flyer-plate" impact test [30]. The procedure employed here generates a pair of shock waves which propagate, at a shock speed U_s, from the cell boundaries toward its center. It should be noted that while the procedure employed involved contraction of the unit-cell at only one of its faces, due to the use of the periodic boundary conditions, a pair of shocks was generated. In other words, it was not possible to generate a single shock while maintaining material continuity (i.e., satisfying the periodic boundary condition). As schematically shown in Fig. 2, these shock waves leave behind a "shocked" material state characterized by a higher material density (as well as internal energy, temperature, stress, particle velocity, and entropy).

The aforementioned procedure for shock-wave generation and the subsequent molecular statics/dynamics analyses are carried out through the use of a Discover input file [28] which is written in a Basic Tool Command Language (BTCL). This enabled the use of a scripting engine that provides very precise control of simulation jobs, e.g., a cell deformation to be carried out in small steps each followed by a combined energy-minimization/molecular-dynamics simulation run.

Problem formulation

The problem addressed in this study involved generation of shock waves of different strengths (using the aforementioned computational cell parameter contraction method), determination of the associated shock-Hugoniot relations and identification and elucidation of the main molecular-level inelastic-deformation/energy dissipation processes taking place at or in the vicinity of the shock front. The procedure for shock-wave generation was presented in the previous section.

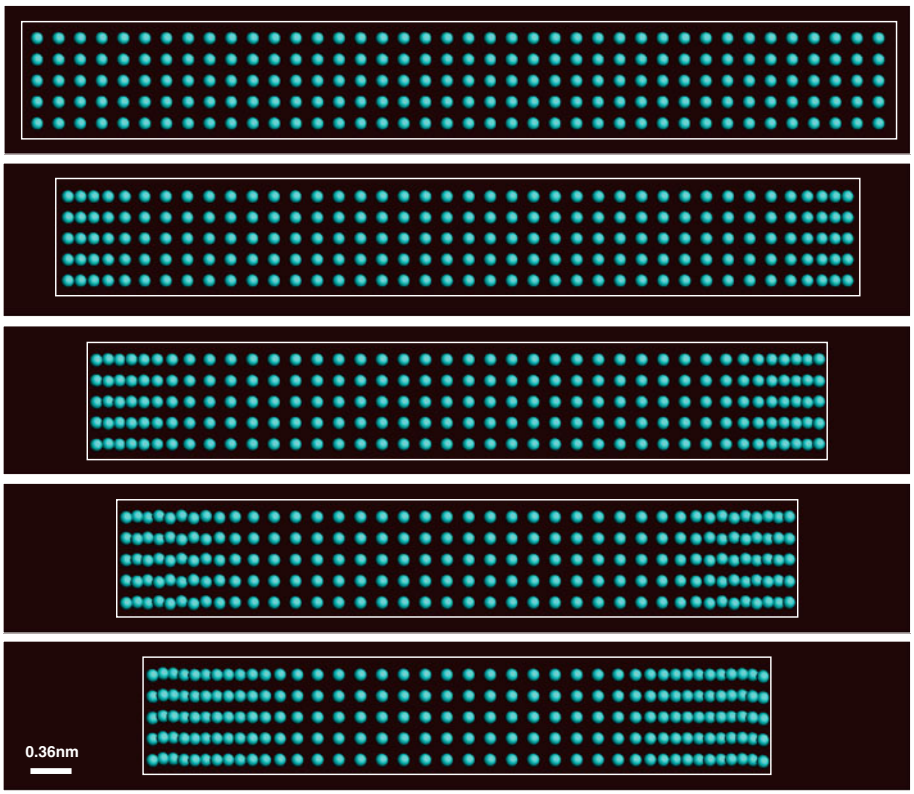

Fig. 2 A schematic of the generation of a pair of shocks in a molecular-level system via the process of computational-cell parameter contraction (Color figure online)

As far as the shock Hugoniot determination is concerned, it entailed the knowledge of the shock-wave profiles (and their temporal evolution) for the axial stress, material density, particle velocity, internal energy, and temperature. The latter are obtained by lumping particles/atoms and their (bond and non-bond) potential and kinetic energy contribution, into fixed-width bins, in the order of their axial coordinates. As will be shown in the next section, two types of bins are used: (a) a Lagrangian-type which is fixed to the initial/reference state of the computational cell and (b) a moving-type which is attached to the advancing shock front.

Identification of the molecular-level inelastic-deformation/energy dissipation processes entailed a close examination of the changes in a material bond structure and topology caused by the passage of the shock.

Results and discussion

Shock-wave observation and structure characterization

An example of the typical results, obtained in this study, pertaining to material molecular-level microstructure/topology evolution caused by a continuous axial contraction of the computational cell is displayed in Fig. 3a–d. The results displayed in these figures clearly reveal the generation of a pair of planar shock waves at the two opposing y–z faces of the computational cell, Fig. 3a, and their subsequent propagation toward the center of the cell, Fig. 3b–d. An approximate location of the center-point of the two shocks is indicated using arrowheads in Fig. 3a–d. The results displayed in Fig. 3a–d show that the shock waves remain fairly planar during their motion. The analysis of shock-wave propagation was terminated at a time which is shorter than the two-shock collision time. However, the analysis can be extended throughout the shock-interaction, which will be done in our future study.

While the results displayed in Fig. 3a–d provide clear evidence for the formation and propagation of a pair of opposing planar shock waves, they do not offer any information about the structure/shape of the shock-wave front or about the state of the (upstream) material swept by the shock. The latter aspects of shock-wave generation and propagation within soda-lime glass are addressed in the remainder of this section and in the subsequent sections.

To reveal the structure/shape of the shock wave, the method of (Lagrangian) bins described in section "shock-wave generation" is employed. In this case, the bins are stationary since they are fixed to in the (initial) reference atomic configuration of the computational cell. Consequently, the same atoms are associated with a given bin throughout the entire molecular dynamics simulation. These bins (with an increased thickness, for clarity) are

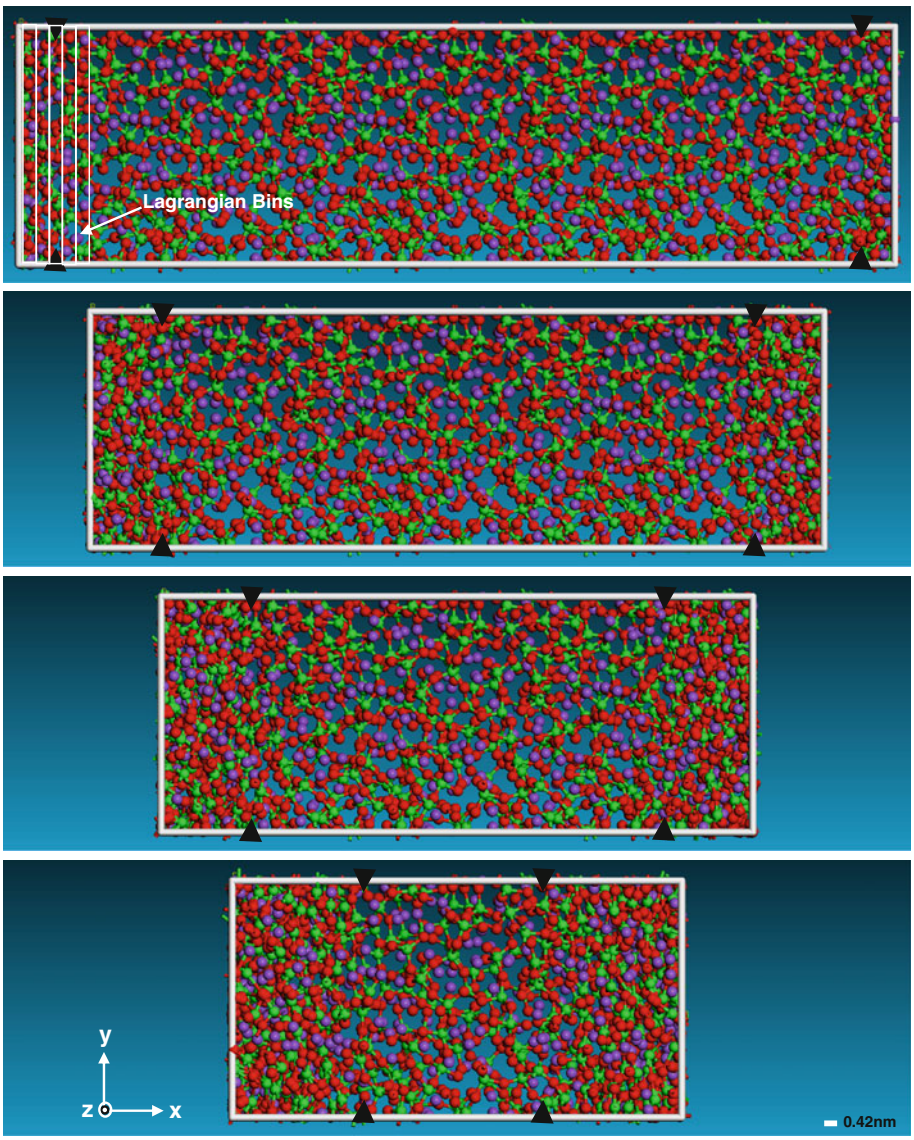

Fig. 3 Temporal evolution of the molecular-level material microstructure accompanying generation and propagation of a pair of planar shocks in soda-lime glass (Color figure online)

depicted in Fig. 3 top part, the initial configuration. Examples of the typical results obtained through the use of this method are displayed in Fig. 4a, b. The results displayed in these figures are obtained under identical conditions except for the rate of axial contraction of the computational cell which is 100% higher in the case of Fig. 4b (750 m/s) relative to Fig. 4a (375 m/s). In these figures, particle velocities at different simulations (i.e., post-shock-wave generation) times, 1 = 60 fs, 2 = 120 fs, 3 = 180 fs, etc. are plotted against the Lagrangian bin center x-location (for the shock propagating to the right, only). Brief examination of the results displayed in Fig. 4a, b reveals that:

(a) two shock waves are generated (only the right-propagating shock is shown though) at the computational cell faces normal to the x-direction. These shocks subsequently propagate toward the computational-cell center;

(b) after a brief transient period, the shocks appear to attain steady wave profiles (i.e., a nearly time-invariant profile within a reference frame which is attached to, and moves with, the shock front). This is demonstrated for the weaker shock case in Fig. 4c in which the shock profile for the curves labeled 3 and 4 in Fig. 4a are redrawn within a moving frame attached to the inflection point of the shock profile; and

(c) both the particle velocity and the shock speed increase with the computational-cell contraction rate. It should be noted that the curves bearing the same numerical label in Fig. 4a, b correspond to the same simulation time.

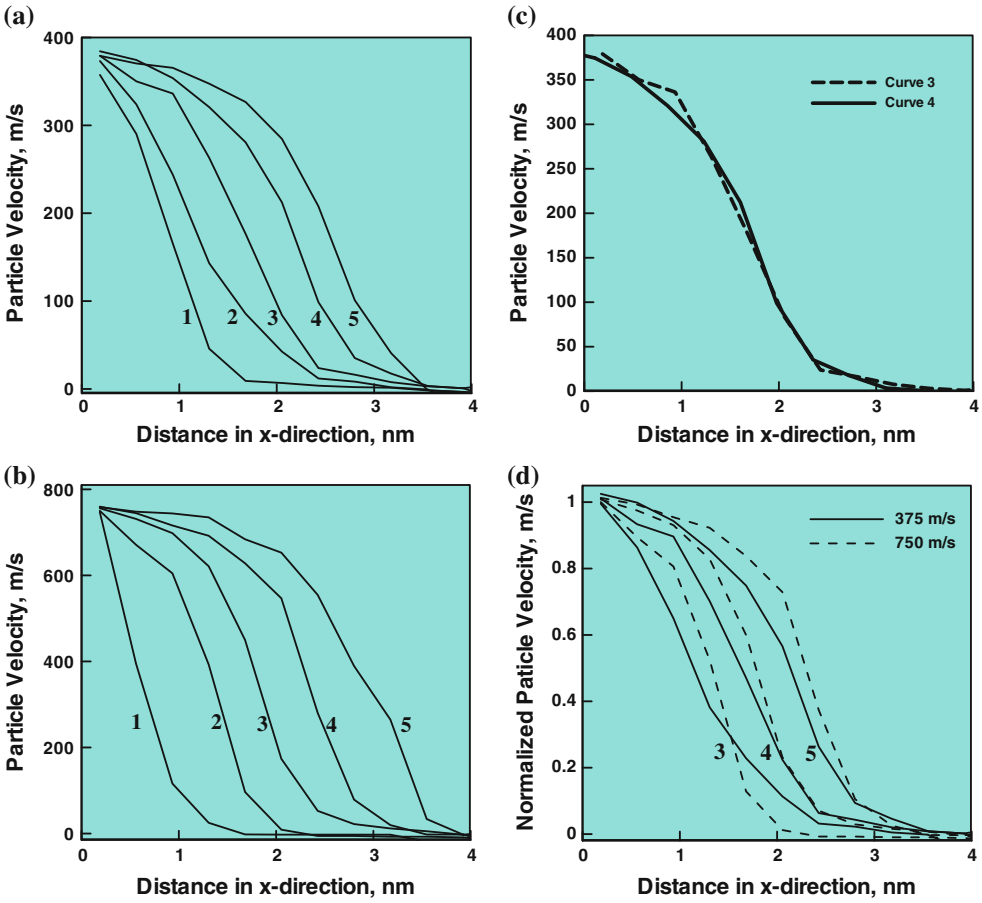

Fig. 4 Temporal evolution of the particle velocity associated with the propagation of two approaching shock waves under the imposed computational cell contraction rate of **a** 375 m/s; and **b** 750 m/s. The simulation time associated with each of the curves is equal to the curve number label multiplied by 60 fs; **c** superposition of the curves 3 and 4 from part **a** suggesting steady nature of the shock wave; and **d** superposition of the curves 3, 4, and 5 from parts **a** and **b** demonstrating that the shock width decreases while shock speed increases with an increase in shock strength. Note that the particle velocities are normalized with respect to the respective maximum value (Color figure online)

It should also be noted that no thermostat was used in the present non-equilibrium molecular dynamics simulations, so that the steady-wave shock profile is a natural consequence of a balance between the continuous supply of momentum to the system (through the continuous computational cell axial contraction) and the observed lateral motion of the atoms in the continuously enlarged upstream material domain swept by the shock. It should be noted that, due to the use of periodic boundary conditions in the lateral directions, despite the fact that the unit cell was constrained in these directions, atoms are free to pass through the computational cell lateral boundaries. In general, the use of a thermostat modifies the ($F = ma$ Newtonian-type) equations of motion solved within the molecular dynamics simulations by the introduction of a (velocity-proportional) viscous-dissipation term. It is well-established that, when shock formation and propagation is analyzed within a continuum framework, the use of a viscous-dissipation term is mandatory for the attainment of a steady-wave shock profile. This fact has often been used as a justification for the use of a (local or global) thermostat within molecular-level simulations of shock-wave formation/propagation. While such practices greatly facilitate the attainment of a steady shock, they cannot be readily defended since shock formation and propagation is generally considered to be an adiabatic (no system/surrounding energy exchange) process due to the near-instantaneous material transition to the shocked state. In addition, shock generation/propagation is a non-isentropic process due to the attendance of various energy dissipation mechanisms. These were the determining factors in the decision to not use a thermostat in this study. Due to the lack of a thermostat, the molecular dynamics simulations employed in this study can be characterized as being of a non-equilibrium type. It is interesting to point out that despite the fact that no viscous-dissipation term was added to the Newton's equations of motion, the results displayed in Fig. 4a, b show some of the defining features of shock-waves when they are analyzed in the continuum-level simulations (in the presence of viscous dissipation). Specifically, a steady shock is generated and the shock width decreases with an increase in the shock strength. This point has been demonstrated in Fig. 4d in which curves labeled 3,4, and 5 from Fig. 4a, b have been re-plotted.

The examination of the results displayed in Figs. 4a–d further reveals that in the weak-to-intermediate shock strength range examined, the observed shock-width is quite small (ca. 2–3 nm). This finding suggests that the dominant energy dissipation processes captured by the molecular-

level simulations are quite weak. As will be shown later, these processes involve changes in the soda-lime glass atomic coordination and in the size of the smallest Si–O rings. In other words, as pointed out by one of the reviewers of this article, viscous dissipation processes with characteristic times at the microsecond time scale are not active in the present simulations. This, in general, only affects the width of the shock profile but not the values of the shocked-material state variables.

Determination of shock-Hugoniot relations

The results presented in Fig. 4a, b reveal the steady-shock profile and can be used to find a functional relationship between the shock speed, U_s, and the particle velocity, u_p. This was done in this study and the results obtained (depicted using discrete symbols) along with their least-square linear fit (depicted as a straight line) are displayed in Fig. 5. Also displayed in Fig. 5 is the corresponding experimental data from [22]. Examination of Fig. 5 reveals that the agreement between the present computational data and their experimental counterparts is fair. In particular, there are two main points of disagreement between the two sets of results: (a) the experimental data in the low particle velocity (i.e., at low stress) region show an anomalous material behavior which is characterized by negative particle-velocity dependency of the shock (or more precisely a smooth wave) speed; and (b) in the high particle-velocity range, the experimental results show a normal material behavior characterized by a positive particle-rate dependency of the shock speed. However, the magnitude of this dependency is somewhat larger than the one predicted by the present computational work. These disagreements reveal that shortcomings/limitations of the present computational approach.

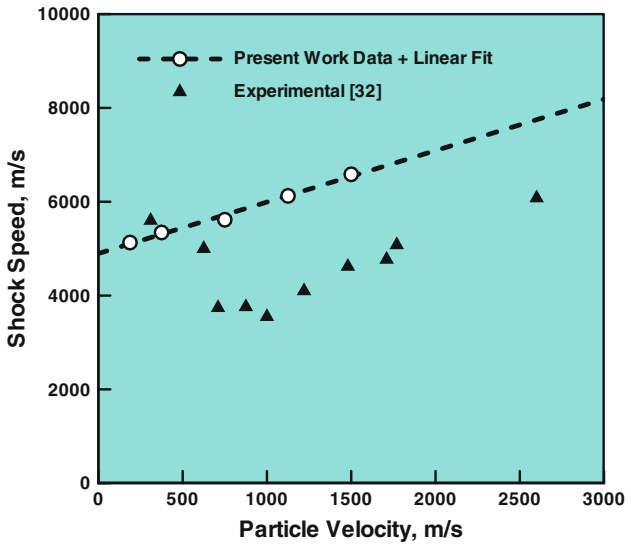

Fig. 5 The Hugoniot relation pertaining to the particle velocity dependence of the shock speed (Color figure online)

The U_s vs. u_p relation mentioned above is a simple projection of the Hugoniot to the U_s–u_p plane. In the case of planar shocks, of interest in this study, the other commonly used Hugoniot relations include: axial stress, t_{11}, vs. density, ρ (or specific volume, $v = 1/\rho$); (mass-based) internal energy density, e, vs. ρ (or v); t_{11} vs. u_p and temperature T vs. ρ (or v). These relations were determined in this study using two distinct methods:

(a) The first method is based on the three so-called jump equations which are defined as [30]:

$$\rho^- U_s = \rho^+ \left(U_s - u_p\right) \tag{2}$$

$$t_{11}^- + \rho^- U_s^2 = t_{11}^+ + \rho^+ \left(U_s - u_p\right)^2 \tag{3}$$

$$e^- + \frac{t_{11}^-}{\rho^-} + 0.5 U_s^2 = e^+ + \frac{t_{11}^+}{\rho^+} + 0.5\left(U_s - u_p\right)^2 \tag{4}$$

These equations relate the known downstream material states (denoted by a superscript "−") and the unknown upstream material states (denoted by a superscript "+") associated with the shock of a given strength (as quantified by the shock speed or the downstream-to-upstream particle velocity jump). These equations are next combined with the previously determined U_s vs. u_p relation and the prescribed (shock-strength defining quantity) U_s or u_p to solve for the unknown upstream material states. It should be noted that this method enables determination of only material mechanical state variables (t_{11}, e, $v(=1/\rho)$, U_s and u_p). To obtain temperature, a separate set of equilibrium *NVE* (E—total energy of the system) molecular dynamics simulations is carried out. In each case, a local computational sub-cell is defined containing only the upstream (shocked) material. The number of particles, the volume of the sub-cell and its total internal energy are all maintained constant. The associated "equilibrium" temperature is then calculated using the time-averages of the atomic velocities (see Eq. 6 below); and

(b) Time averages of the atomic positions, r_i, velocities, v_i, and interaction forces, f_i (i is the atomic label) are used to compute the unknown, local (bin-based) thermo-mechanical quantities using the following standard statistical thermodynamic relations:

$$\rho = \frac{1}{V_{\text{bin}}} \left[\left(\sum_{i=1}^{N_{\text{bin}}} m_i \right)_{\text{avg}} \right] \tag{5}$$

$$T = \left(\frac{1}{3N_{\text{bin}}k_b} \left[\sum_{i=1}^{N_{\text{bin}}} m_i v_i . v_i \right] \right)_{\text{avg}} \quad (6)$$

$$t_{11} = \frac{1}{V_{\text{bin}}} \left(N_{\text{bin}} k_b T + \sum_{i=1}^{N_{\text{bin}}} r_i \otimes f_i \right)_{\text{avg}} \quad (7)$$

$$E = \left(E_{\text{Total}} + \frac{1}{2} \left(\sum_{i=1}^{N_{\text{bin}}} m_i v_i . v_i \right) \right)_{\text{avg}} \quad (8)$$

where subscript avg denotes time averaging, N_{bin} and V_{bin} are the number of atoms within and the volume of the bin, respectively, k_{b} is the Boltzmann's constant, E_{Total} is the potential energy of a system in a given configuration, while "•" and "⊗" indicate dot product and tensorial product operators, respectively. It should be noted that the stress relation, Eq 7 is a particular representation of the standard virial-based stress equation [31].

It should be noted that, in this case, the bins were defined within a reference frame which is attached to (and moves with) the steady-shock front. Clearly, in this case different atoms may reside within a given bin at different simulation times. On the other hand, the bins correctly collect the information about the atoms (temporarily) residing in a given segment of the steady-shock profile. In other words, time averages are calculated not for a fixed assembly of atoms, but rather for a transient set of atoms associated with a given moving bin. It should be also noted that since one of the main objectives of this study was determination of the Hugoniot relations, only the data pertaining to the bins located in the fully shocked upstream region are collected and analyzed (for different shock-strength conditions). In other words, the data collected by the bins located within the shock profile and downstream of the shock are ignored.

The results of these two procedures are displayed in Fig. 6a–d. In each of these figures, two cases are shown and labeled as "Method (a)" or "Method (b)" to indicate the method used for generation of the corresponding results. The results displayed in these figures show that, in the weak-shock regime, method (a) consistently over-predicts (by as much as 100%) the values of the material state variables relative to method (b). This relative difference continuously diminishes with shock strength so that in the

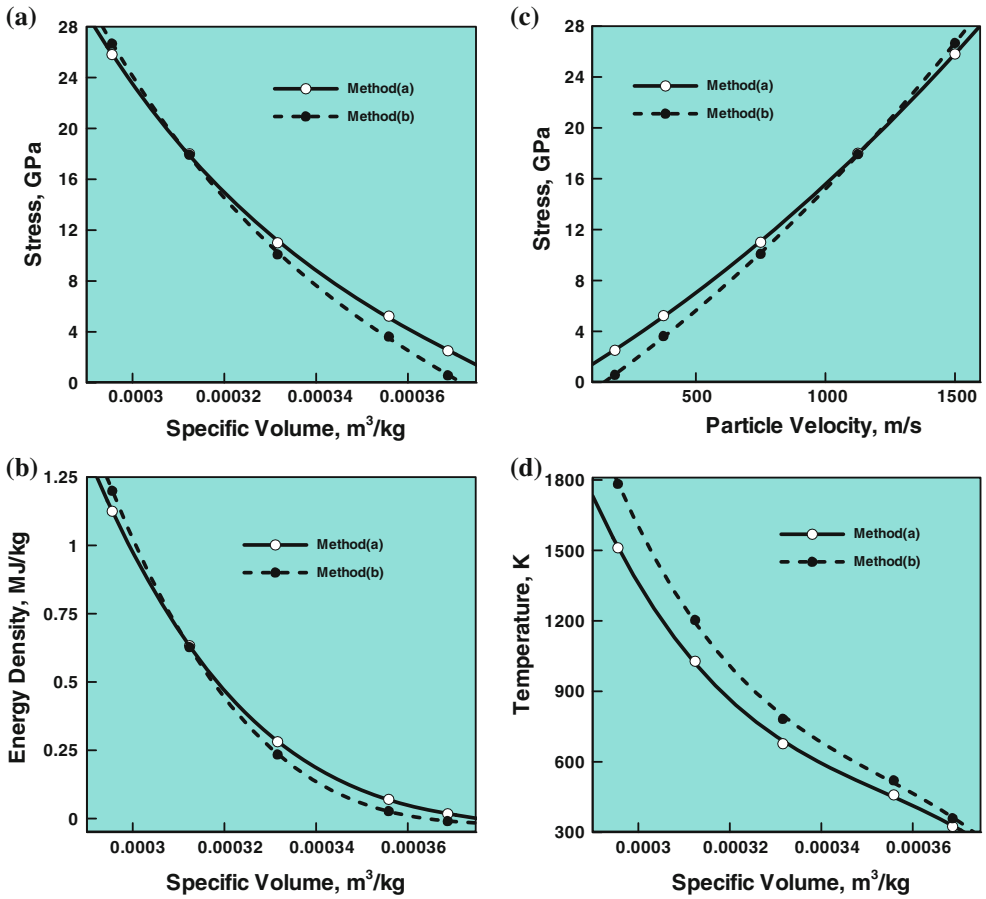

Fig. 6 **a** Axial stress versus specific volume; **b** energy versus specific volume; **c** axial stress versus particle velocity Hugoniot relations. Please see text for explanation of the "Method (a)" and "Method (b)" (Color figure online)

strong-shock regime the predictions of the two methods are different by less than 10%.

The Hugoniot relations displayed in Figs. 5 and 6a–d are typically used within a continuum-level computational analysis of shock-wave generation/propagation in two ways:

(a) They are directly used in the analysis of shock-wave propagation under uniaxial strain conditions [32, 33]; and
(b) Alternatively, they can be used to derive a continuum-level material model which is consistent with the material mechanical response under high-rate, large-strain, high-pressure conditions. Such a model is subsequently used in general three-dimensional, non-linear dynamics computational analyses [22].

In our recent work [6], it was shown that the Hugoniot relations can be generated by converting the corresponding isotherms (obtained via quasi-static, molecular-level mechanical tests). This procedure was found to be associated with a number of challenges (e.g., a particular form of the equation of state had to be assumed, several material properties/relations had to be assessed independently, etc.). Most of these challenges were not encountered in this study since the Hugoniot relations are derived more directly from the molecular-level computational results.

Shock-induced material-state changes

The results presented and discussed in the previous sections clearly revealed the formation and propagation of planar shocks in soda-lime glass and enabled formulation of the appropriate shock-Hugoniot relations. In the present section, a more detailed investigation is carried out of the molecular-level material microstructure in the wake of a propagating planar shock.

It should be first realized that the analysis of material microstructure and its evolution due to shock loading in soda-lime glass is quite challenging due to the absence of a crystal structure in this material. Namely, when molecular-level simulations of shock generation/propagation are carried out in (nearly perfect) single crystal solids [17, 20], the presence of a crystal lattice greatly facilitates the investigation of deviations from the long range order (i.e., formation of various point, line and planar defects) and the nature of the associated inelastic deformation processes. Soda-lime glass is, on the other hand, an amorphous material in its initial condition and remains so after being subjected to shock loading. To address the challenge of material microstructure characterization and its changes resulting from shock loading, the following microstructural parameters were monitored: (a) the random network X parameter. The R parameter was not monitored since it is microstructure-insensitive while Y parameter was not monitored since $X + Y = 4.0$ in pure silicate glasses (like soda lime glass); (b) the Si-atom average coordination number(i.e., bonding structure); (c) the size of the smallest Si–O ring; and (d) the material's average density.

In the case of single-crystalline solids, previous molecular-level shock-wave formation/calculation work (e.g., [17, 20]) established that the steady-wave condition is attained not as a result of (velocity-dependent) viscous dissipation (as is the case for shocks in fluids), but rather as a result of inelastic deformation (permanent slippage of crystal planes and the formation of crystal defects) and phase transformation processes. The microstructural parameters identified above are used to characterize the type and the extent of these processes.

X parameter evaluation

In general, changes in the X parameter are the result of competition between Si and O bond breaking processes (increases the average number of non-bridging oxygens per un-shocked material polyhedron) and the processes which lead to an increase in Si-atom coordination number (decrease the X parameter value). Since the instances of Si-atom coordination-number increase are found to greatly out-number the Si–O bond-breaking instances, the value of the X parameter has been found to decrease by 5–10% from its equilibrium value (=0.81).

Si-atom average coordination number

Examination of the material microstructure in the shock wake revealed that the Si-atom average coordination number increases from its initial value of 4.0 by 2–3%. An example of the shock-loading induced increase in Si-atom coordination number is depicted in Fig. 7a–d. To aid in visualization/interpretation of the microstructural/topological changes experienced by soda-lime glass during shock loading, only a 20–30 atom exemplary region of the upstream material is analyzed in these figures. In addition, sodium cations are not displayed.

In Fig. 7a, c, x–y and y–z projections are given of the material region under consideration in its initial state. The corresponding projections for the same material region after the passing of a shock are displayed in Fig. 7b, d. For improved clarity, three silicon atoms are highlighted in green. To make apparent the Si-atom coordination-number increase, one of the Si atoms is labeled as "*Si*" along with the oxygen atoms bonded to it. It is clear that the silicon atom in question was initially four-fold coordinated and it became five-fold coordinated upon the passage of the shock.

It should be noted that the molecular-level microstructural changes described above are a manifestation of the

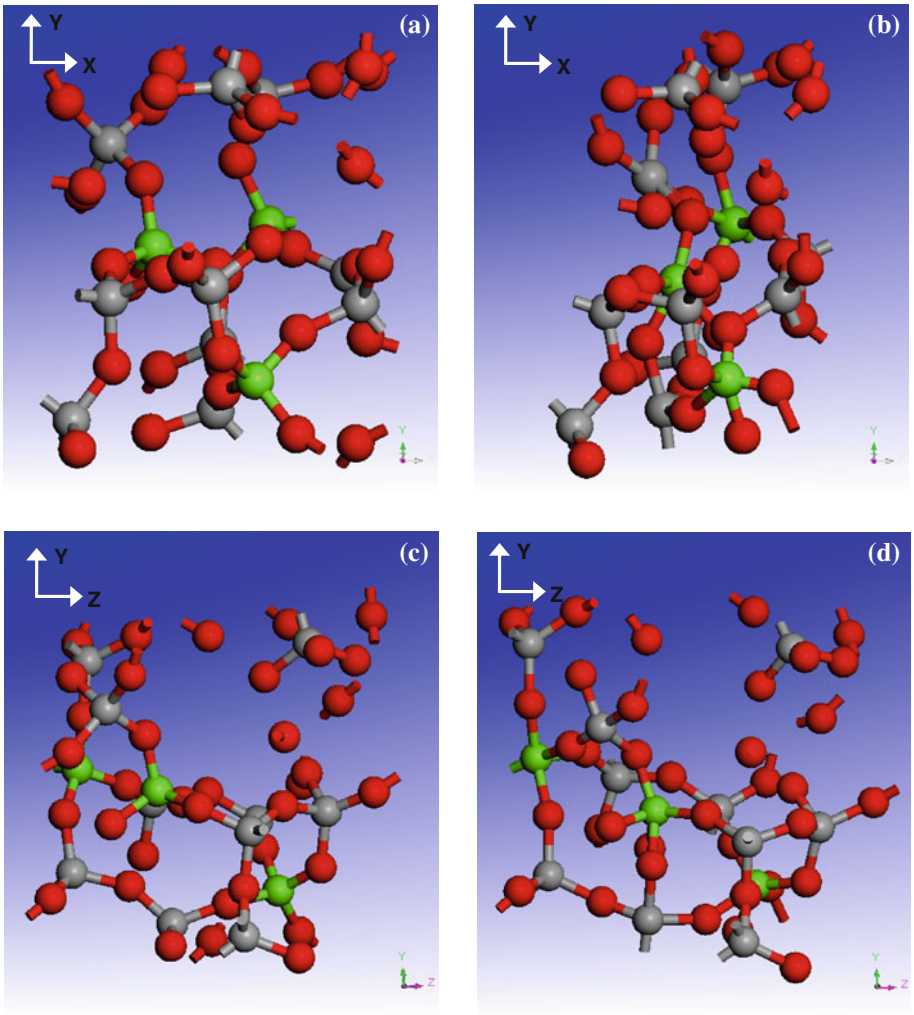

Fig. 7 Development of five-fold coordinated silicon atoms in soda-lime glass under shock loading: **a** material initial state, *x*–*y* projection; **b** post-shock state of the same material region as in (**a**); **c** and **d** *y*–*z* projection of (**a**) and (**b**), respectively (Color figure online)

transition of soda-lime glass to a state that is energetically favored at high shock-induced stresses (large densities). This finding is consistent with the experimental observation of Alexander et al. [22] who reported the formation of stishovite-like domains containing six-fold coordinated silicon atoms in soda-lime glass at ca. 30 GPa shock-induced axial stress levels.

Si–O ring minimum size

It should be first noted that a comprehensive statistics-based Si–O ring minimum-size analysis is quite complicated and is beyond the scope of this study. Such an analysis will be carried out in our future work. Instead, only a qualitative analysis of the molecular-level shocked material microstructure is carried out here to obtain evidence for the potential reduction in the minimum size of the Si–O rings. An example of two Si–O rings each containing five silicon atoms found in the as-shocked material is shown in Fig. 8. For improved clarity, these rings are highlighted in purple and yellow. Similar rings were not observed in the initial un-shocked material. This finding was reconfirmed using different (yet, all equilibrium) initial molecular structures. Thus, this study suggests that shock loading causes a reduction in the minimum Si–O ring size.

Material's average density

It should be also recognized that shock loading leads to a permanent 2–4% (shock strength-dependent) increase in the material density. This material densification process along with the aforementioned processes leading to an increase in the silicon-atom coordination and smaller Si–O ring formation are all associated with energy absorption/dissipation and, hence, are expected to play an important role in the blast/ballistic impact mitigation potential of soda-lime glass.

Final remarks

Within this study, molecular-level computational methods are employed to study various phenomena accompanying

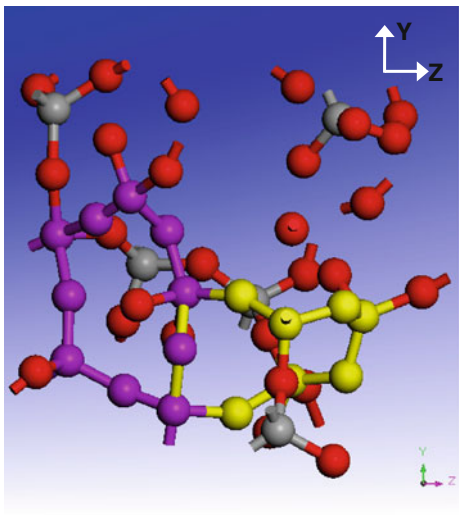

Fig. 8 Observations of smaller Si–O rings (containing five Si atoms) in the as-shocked soda-lime glass. Similar small-size rings Si–O rings were not observed in the initial/un-shocked material state. The rings in question have been highlighted for clarity (Color figure online)

shock-wave generation and propagation in soda-lime glass. It should be noted that this study does not suggest that molecular-level analyses of shock generation and propagation should replace the corresponding continuum-level (hydrodynamic) analyses. The latter are far better suited (and feasible) for studying the behavior of real-life engineering systems (e.g., vehicle windshield subjected to blast impact). Rather, the present approach is highly beneficial relative to the identification and characterization of the nanoscale phenomena/processes taking place at the shock front. Once these phenomena/processes are well understood and characterized (a formidable task) the knowledge gained can be used to formulate (and parameterize) more physically based material models suitable for use in continuum-level analyses.

Summary and conclusions

Based on the results obtained in this study, the following summary remarks and main conclusions can be drawn:

1. Various phenomena accompanying the formation and propagation of a planar shock-wave within soda-lime glass, a material commonly used in transparent armor applications, are investigated using molecular-level computational methods.
2. The results obtained show that even without the use of a viscous-dissipation-based thermostat, a steady-wave planar shock profile can readily be established in this material.
3. The time-averaged results pertaining to the atomic positions, velocities and interaction forces are used to construct the appropriate shock–Hugoniot relations, the relations which define the locus of stress, energy density, mass density, temperature, and particle velocity in soda-lime glass swept by a shock propagating at a given speed.
4. Detailed examination of the molecular-level microstructure evolution in the shock-wave wake is carried out to identify the nature of energy-absorbing and shock-wave spreading mechanisms. The results revealed that shock loading causes extensive changes in atomic coordination and the bond structure as well as a 2–4% (shock strength-dependent) density increase. Specifically, the atomic coordination of many silicon atoms has been found to increase from four to five and numerous smaller Si–O rings are observed. These processes are associated with substantial energy absorption and dissipation and are believed to greatly influence the blast/ballistic impact mitigation potential of soda-lime glass.

Acknowledgements The material presented in this article is based on study supported by the U.S. Army/Clemson University Cooperative Agreements W911NF-04-2-0024 and W911NF-06-2-0042 and by an ARC-TARDEC research contract.

References

1. Strassburger E, Patel P, McCauley W, Templeton DW (2005) In: Proceedings of the 22nd international symposium on ballistics, November 2005, Vancouver, Canada
2. Fink BK (2004) AMPTIAC Q 8(4):991
3. Grujicic M, Pandurangan B, Coutris N, Cheeseman BA, Fountzoulas C, Patel P, Strassburger E (2008) Mater Sci Eng A 492(1): 397
4. Grujicic M, Pandurangan B, Bell WC, Coutris N, Cheeseman BA, Fountzoulas C, Patel P (2009) J Mater Eng Perform 18(8): 1012
5. Grujicic M, Pandurangan B, Coutris N, Cheeseman BA, Fountzoulas C, Patel P (2009) Int J Impact Eng 36:386
6. Grujicic M, Bell WC, Glomski PS, Pandurangan B, Cheeseman BA, Fountzoulas C, Patel P (2010) J Mater Eng Perform. doi: 10.1007/s11665-010-9774-2
7. Woodcock LV, Angell CA, Cheeseman P (1976) J Chem Phys 65:1565
8. Valle RGD, Venuti E (1996) Phys Rev B 54(6):3809
9. Trachenko K, Dove MT (2002) J Phys Condens Matter 14:7449
10. Liang Y, Miranda CR, Scandolo S (2007) Phys Rev B 75:024205
11. Nghiem B (1998) PhD thesis, University of Paris 6, France
12. Denoual C, Hild F (2002) Eur J Mech Solids A 21:105
13. Yazdchi M, Valliappan S, Zhang W (1996) Int J Numer Methods Eng 39:1555
14. Hild F, Denoual C, Forquin P, Brajer X (2003) Comput Struct 81:1241
15. Holmquist TJ, Templeton DW, Bishnoi KD (2001) Int J Impact Eng 25:211
16. Camacho GT, Ortiz M (1996) Int J Solids Struct 33(20–22):2899
17. Holian BL, Straub GK (1598) Phys Rev Lett 43:1979
18. Straub GK, Schiferl SK, Wallace DC (1983) Phys Rev B 28:312

19. Klimenko VY, Dremin AN (1978) In: Breusov ON et al (eds) Detonatsiya, Chernogolovka. AkademiiNauk, Moscow, p 79
20. Holian BL, Hoover WG, Moran B, Straub GK (1980) Phys Rev A 22:2498
21. Kingery WD, Bowen HK, Uhlmann DR (1976) Introduction to ceramics, 2nd edn. Wiley, New York, p 91
22. Alexander CS, Chhabildas LC, Reinhart WD, Templeton DW (2008) Int J Impact Eng 35:1376
23. Sun H (1998) J Phys Chem B 102:7338
24. Sun H, Ren P, Fried JR (1998) Comput Theor Polym Sci 8(1/2):229
25. http://www.accelrys.com/mstudio/msmodeling/visualiser.html
26. http://www.accelrys.com/mstudio/msmodeling/amorphouscell.html
27. Grujicic M, Sun YP, Koudela KL (2007) Appl Surf Sci 253:3009
28. http://www.accelrys.com/mstudio/msmodeling/discover.html
29. Theodorou DN, Suter UW (1986) Macromolecules 19:139
30. Davison L (2008) Fundamentals of shock wave propagation in solids. Springer, Berlin, Heidelberg
31. Allen MP, Tildesley DJ (1994) Computer simulations of liquids. Clarendon Press, New York
32. Grujicic M, Bell WC, Pandurangan B, Glomski PS (2010) J Mater Eng Perform. doi: 10.1007/s11665-010-9724-z
33. Grujicic M, Bell WC, Pandurangan B, He T (2010) Mater Des 31(9):4050